Measurement of the Inclusive Jet Cross Section in $\bar{p}p$ Collisions at $\sqrt{s} = 1.96\,\text{TeV}$

The DØ Collaboration
URL: http://www-d0.fnal.gov

(Dated: May 10, 2006)

We present a new preliminary measurement of the inclusive jet cross section in $\bar{p}p$ collisions based on a integrated luminosity of about $0.8\,\text{fb}^{-1}$. The data were acquired using the DØ detector between 2002 and 2005. Jets are reconstructed using an iterative cone algorithm with radius $R_{\text{cone}} = 0.7$. The inclusive jet cross section is presented as a function of transverse jet momentum and rapidity. Predictions from perturbative QCD in next-to-leading order, plus threshold corrections in the 2-loop accuracy describe the shape in p_T.

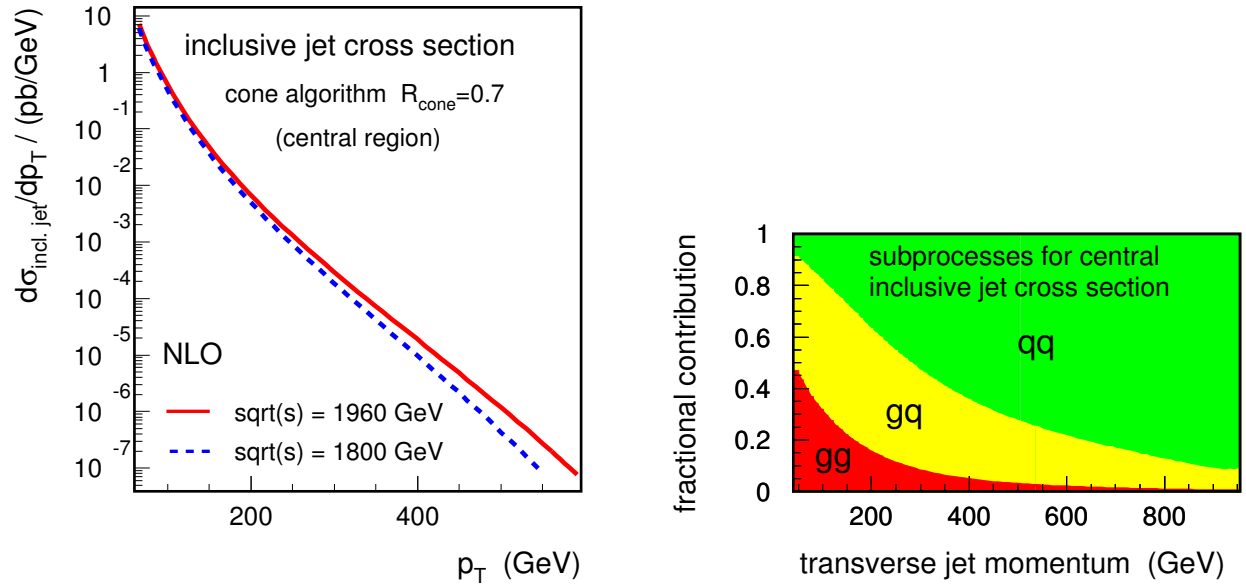*Preliminary Results for Spring 2006 Conferences*

FIG. 1: The NLO pQCD predictions using the CTEQ6.1M parametrization [1] for the central inclusive jet cross section in $p\bar{p}$ collisions at two different center-of-mass energies $\sqrt{s}$ (left) and the fractional contributions from different partonic subprocesses (right).

The production of particle jets in hadron collisions is described by the theory of Quantum Chromodynamics (QCD). When the transverse jet momentum with respect to the hadron beam direction (p_T) is large, the contributions from long-distance physics processes with low p_T are small and the production rates of jets can be predicted by perturbative QCD (pQCD). The inclusive jet cross section in $p\bar{p}$ collisions at large p_T is directly sensitive to the strong coupling constant (α_s) and the parton density functions (PDFs) of the proton. Furthermore, potential deviations from the pQCD prediction at high p_T, not explained by PDFs or α_s, may indicate new physics beyond the Standard Model. In Run II of the Fermilab Tevatron Collider the center-of-mass energy was increased to $\sqrt{s} = 1.96$ TeV, as compared to $\sqrt{s} = 1.8$ TeV in Run I. The moderate increase in the center-of-mass energy, however, leads to a significant increase in the inclusive jet cross section at high p_T. At $p_T = 500$ GeV/c the cross section is expected to increase by almost 300% as shown in Figure 1 using the CTEQ parametrization [1] (left). Together with the increased integrated luminosity in Run II this extends the accessible p_T range and allows to test pQCD at previously unexplored energies. The expectation of the fractional contributions to the inclusive jet cross section from different partonic subprocess are displayed in Fig. 1 (right), and one of the purposes of the measurement described in this note will be to get a better constraint of these fractions. It is seen that at low p_T the jet cross section is dominated by gluon-gluon and gluon-quark induced processes, while at high p_T quark-quark scattering gives the dominant contribution. At p_T=500 GeV/c, however, there is still a contribution of $\approx 30\%$ from gluon-quark scattering, and thus some sensitivity to the gluon density in the proton which is here probed at large momentum fractions $x \approx 0.5$. The measurement is sensitive to quark and gluon contributions, but is especially interesting to gluon contribution at high-x which can be furher constrained using this data.

In this note we present an updated preliminary measurements of the inclusive jet cross section at $\sqrt{s} = 1.96$ TeV, based on a data sample corresponding to an integrated luminosity of about L = 0.8 fb^{-1}. Data were acquired with the upgraded DØ detector [2] between 2002 and 2005 in Run II of the Fermilab Tevatron. Events used in this analysis were triggered by single jet triggers, based on energy deposited in calorimeter towers. Data selection was based on run quality, event properties (missing-$E_T < 0.7 \cdot p_T$ to remove mostly cosmic background, primary vertex $z < 50$ cm to improve jet p_T resolution), and jet quality criteria.

This measurement complements earlier inclusive jet cross section measurements by CDF [3] and Tevatron Run I [4, 5].

Jets were defined by the "Run II cone algorithm" [6] which combines objects (calorimeter towers in the experiment, stable particles in a Monte Carlo event generator, or partons in a pQCD calculation) within a cone of radius $R_{cone} = 0.7$ in rapidity, y, and azimuth, ϕ, around the cone axis using the "E-scheme" (adding the four-vectors). Every object serves as a seed which is used as the cone axis for a new proto-jet. The objects inside the cone radius around the axis are combined into a jet and this procedure is iterated until the jet axis coincides with the cone axis. The four-vectors of all objects are used as seeds in the first stage of the iterative procedure. The algorithm is re-run using the midpoints
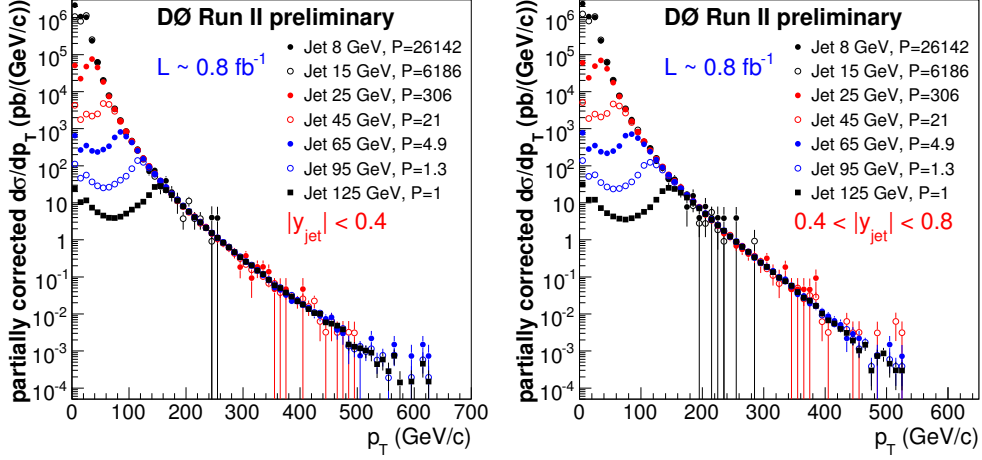
FIG. 2: The inclusive jet cross section in two rapidity ranges, measured with different jet triggers at different p_T thresholds.

between pairs of jets as additional seeds (this makes the procedure infrared safe). Jets with overlapping cones are merged if the overlap area contains more than 50% of the p_T from the lower p_T jet, otherwise the objects in the overlap region are assigned to the nearest jet.

The inclusive jet cross section is measured in two central rapidity regions $|y_{jet}| < 0.4$ and $0.4 < |y_{jet}| < 0.8$. We note that the data are corrected for underlying events when the jet energy scale is computed. The jet energy scale corrects for "offset" energies measured using zero-bias events which correspond to uranium noise (jets are measured with a liquid Argon-Uranium calorimeter), pile-up effects and underlying events because these effects cannot be distinguished experimentally. Data are corrected for the jet energy scale, selection efficiencies, and for migrations due to p_T resolution. The jet energy scale was determined by minimizing the missing transverse energy in isolated photon plus jet events. The detector pseudorapidity dependence of the jet energy scale was determined using both dijet and isolated photon plus jet events. Spectra in p_T are fit, in an iterative procedure, with parameterized ansatz functions and folded with resolutions determined from data. Ratios of the original to the folded ansatz functions are used to correct the data for folding of resolution effects. Another method using a folded version of PYTHIA [7] using the jet p_T and y resolutions was used to cross check the results.

The contributions from different triggers to the partially corrected jet p_T spectra are shown in Fig. 2 (no corrections for migrations are applied at this stage). Once the jet p_T reaches the trigger turn-on point, the spectrum follows the p_T spectra of the triggers with lower thresholds.

As we mentioned, two different methods have been used to unfold the data. The first method uses a four parameter ansatz function given in Formula 1 convoluted with the jet p_T resolution measured directly in data:

$$f(N, \alpha, \beta) = N \left(\frac{p_T}{p_{T0}} \right)^{-\alpha} \left(1 - \frac{2 \cosh(y_{jet,min}) p_T}{\sqrt{s}} \right)^{\beta} \exp(-\gamma p_T), \tag{1}$$

with $p_{T0} = 1$ GeV/c and $y_{jet,min}$ chosen to be the minimum jet rapidity in the respective bin ($y_{jet,min} = 0.0$ or $y_{jet,min} = 0.4$). The second method uses PYTHIA events and a fast simulation of the resolution in jet rapidity and transverse momentum. Results are shown in Fig. 3 and found to be in good agreement between both methods. We also note the good description of the data by the chosen ansatz. The decrease of the correction factor towards low p_T is explained by the poor p_T resolution at low p_T.

The dominant uncertainty in the cross section measurement is due to the jet energy scale. Fig. 4 shows the relative variation of the jet cross section when the jet energy scale is varied by one standard deviation in both directions. In the photon plus jet sample that was used to calibrate jet energies, jets reach energy up to ≈ 300 GeV. Therefore the uncertainties are largest at highest p_T. The size of the jet energy scale statistical uncertainties will decrease further in a near future. The jet energy scale used for this measurement was computed using γ+jet events in a statistically limited sample of about 150 pb^{-1} and the final determination of jet energy scale corrections using the full data set of about 1 fb^{-1} is being finalized. Further sources of uncertainty are due to the data selection and trigger efficiency, different correction for migrations and the jet p_T resolution. In addition, the luminosity measurement has an uncertainty of 6.5%.
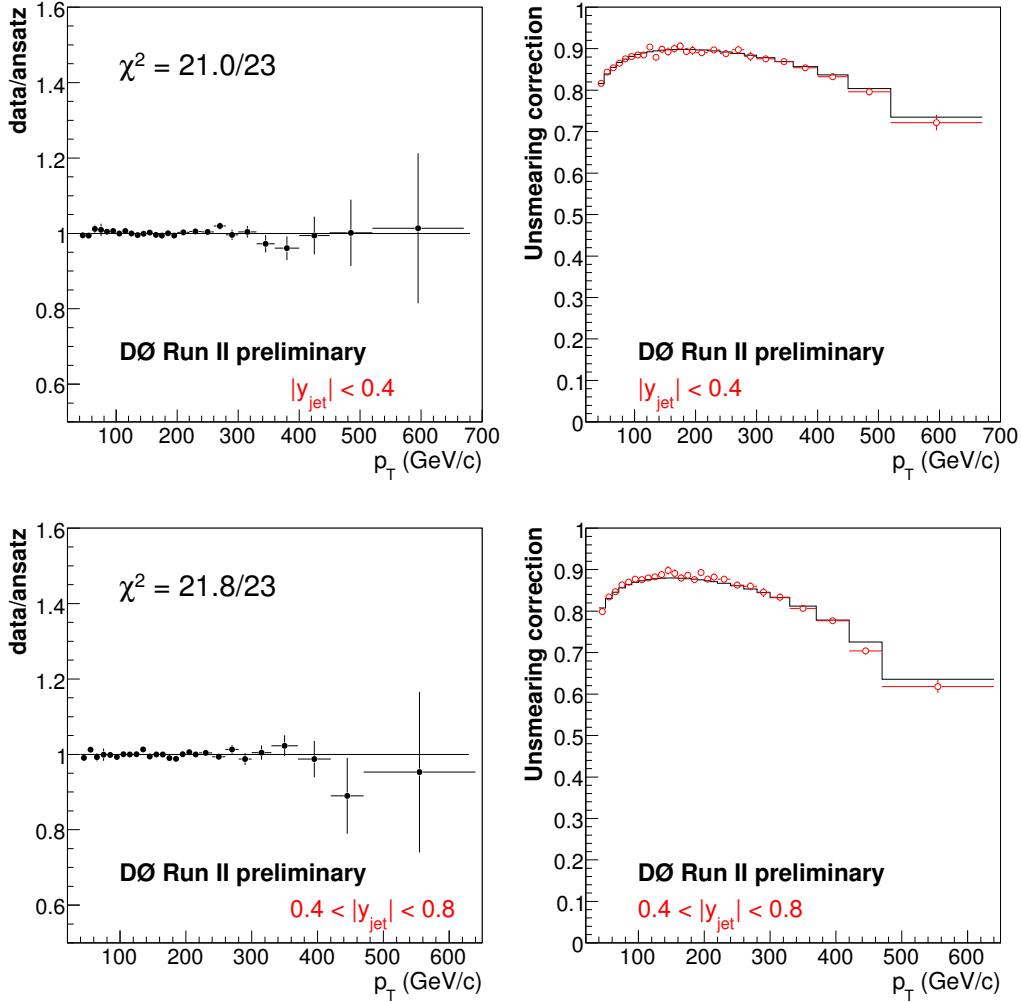
FIG. 3: Unfolding corrections in the two central rapidity bins. Left plots show relative difference between the data and folded ansatz function (Eq. 1). Right plots display the derived unfolding correction from the ansatz function (solid lines) and from folding Pythia jets (open circles) with the p_T resolution obtained directly from data.

In the following, we compare the measurement with the next-to-leading (NLO) pQCD predictions with threshold corrections in the 2-loop accuracy [11]. The NLO pQCD predictions are computed using the program fastNLO [9] based on NLOJET++ [8] and the PDFs from CTEQ6.1M [1] and MRST2004 [10]. The renormalization and factorization scales are set to the transverse momenta of the individual jets $\mu_R = \mu_F = p_T$. A variation by a factor of two is considered to be a part of the theoretical uncertainty. The Run II cone algorithm used in this analysis is infrared safe, therefore allowing to use exactly the same jet algorithm in the calculation that is used in the experimental measurement. This avoids the ambiguities present in the Run I measurements where the jet definition was not infrared safe and an $R_{\rm sep}$ parameter was introduced in the theory calculation which was not matched to the experimental algorithm.

It is known that the phase space limitations on gluon emission as one goes to large transverse momentum and large rapidity can lead to potentially large contributions to the jet inclusive cross sections. Such corrections have been computed using threshold resummation techniques. These calculations have shown that the two loop contributions to the next-to-next-leading-logarithm are 5–15% [11] and are included in our predictions, except where noted.

Recall that the cross sections are corrected for underlying events. The contributions from soft ("non-perturbative") processes to the jet cross section are studied in Fig. 5. Using the PYTHIA [7] model we investigate the relative effects from hadronization as a function of p_T in two regions of rapidity. Hadronization corrections are here defined as the ratio of the jet cross section after and before hadronization. The study has been redone using the HERWIG [13] model
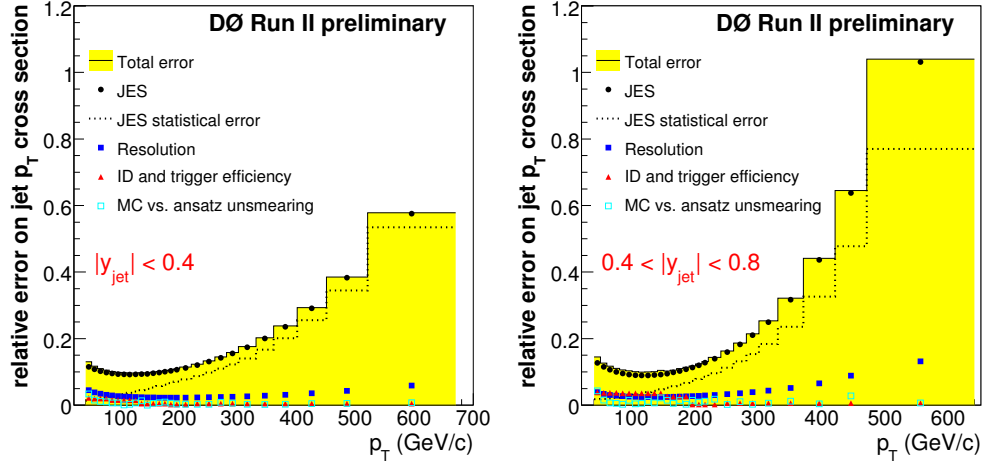
FIG. 4: Relative error on inclusive jet cross section connected to Jet Energy Scale uncertainties (black points, the largest uncertainty by far), Jet Energy Scale statistical uncertainty only (dashed line), jet p_T resolution in blue squares, jet trigger and cut efficiency in red triangles, and two different method of unfolding in green squares.
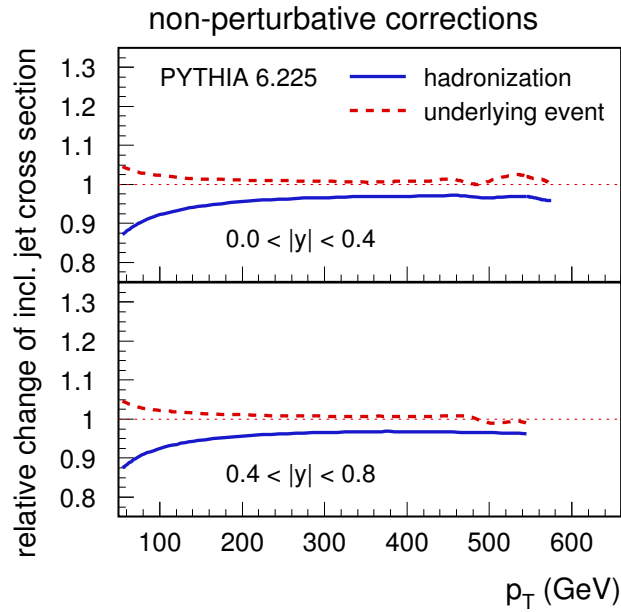

FIG. 5: The size of non-perturbative corrections for the inclusive jet cross sections is displayed as estimated by PYTHIA. The relative changes of the cross section due to hadronization (line) and underlying event (dashed line) are shown as a function of p_T in two rapidity regions.

and the results are consistent with the PYTHIA results. The pQCD predictions have been corrected for hadronization effects using PYTHIA.
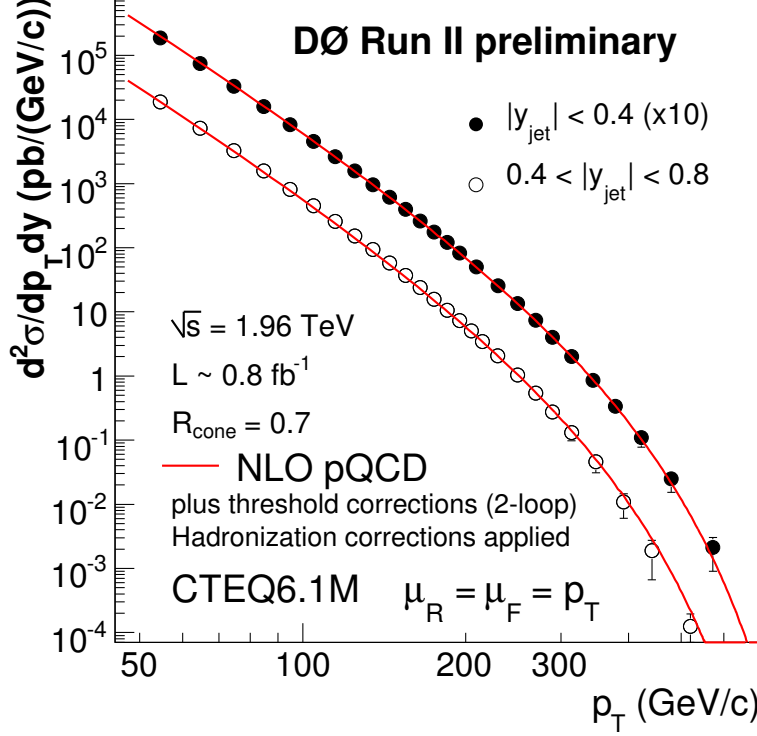
FIG. 6: The inclusive jet cross section, measured in two regions of jet rapidity. Error bars show the total measurement uncertainty. The data at $|y_{jet}| < 0.4$ are scaled by a factor of 10 for presentation purposes. The predictions from pQCD are corrected for hadronization effects and are overlaid on the data as lines.

The preliminary results of the measurement are shown in Fig. 6 as a function of p_T in two regions of rapidity. The data have been scaled to theory at $p_T = 100$ GeV/c for $|y_{jet}| < 0.4$ to remove luminosity uncertainties. The jet cross section at larger rapidity falls more steeply above $p_T = 300$ GeV/c than in the central region. The predictions from pQCD are overlaid on the data as red lines.

The ratio of data and theory is shown in Fig. 7. The systematic experimental uncertainties are displayed as a band; the uncertainty of the pQCD prediction (with and without threshold corrections) due to the choice of the renormalization and factorization scales is displayed by the dashed and dotted lines in Fig.9; the NLO pQCD prediction without threshold corrections is overlayed as a dash-dotted line in Fig. 7. The uncertainties of the theory prediction due to the PDF uncertainties have been determined using the 40 PDF sets from CTEQ6.1 [1], corresponding to up and down variations of the 20 parameters in the PDF fit. The resulting uncertainties are indicated in Fig. 7 by the dashed lines; they show a strong increase with p_T, especially at larger rapidities. The pQCD results for MRST2004 [10] and Alekhin2002 [12] PDFs are shown as the dotted and dashed lines in Fig. 8, respectively.

The event with the highest p_T jet in the data sample is shown in Fig. 10. The leading jet has $p_T = 624$ GeV/c and is balanced in p_T by a second jet which opposite in azimuthal angle. The invariant mass of the dijet system is $M_{jj} = 1.22$ TeV/c^2. The detailed information is given in the table in Fig. 10.

The theoretical predictions are in good agreement with the data over the whole p_T range in both rapidity regions. Let us note that the high-p_T different behavior of the cross section in the two rapidity bins is mainly due to statistical effects in jet energy scale corrections (we showed in Fig 4 that the main error is statistical at high p_T). Therefore, there is no correlation between jet energy scale corrections in the two y bins at high jet transverse momentum. The experimental uncertainties are now competitive with the ones from the proton PDFs, and these data will allow to further constrain the high-x gluon in particular. The high-p_T uncertainty will be further reduced using the full statistics available to extract the jet energy scale.

Acknowledgments

We thank the staffs at Fermilab and collaborating institutions, and acknowledge support from the Department of Energy and National Science Foundation (USA), Commissariat à L'Energie Atomique and CNRS/Institut National de Physique Nucléaire et de Physique des Particules (France), Ministry for Science and Technology and Ministry for Atomic Energy (Russia), CAPES, CNPq and FAPERJ (Brazil), Departments of Atomic Energy and Science and Education (India), Colciencias (Colombia), CONACyT (Mexico), Ministry of Education and KOSEF (Korea), CONICET and UBACyT (Argentina), The Foundation for Fundamental Research on Matter (The Netherlands), PPARC (United Kingdom), Ministry of Education (Czech Republic), Natural Sciences and Engineering Research Council and West-Grid Project (Canada), BMBF (Germany), A.P. Sloan Foundation, Civilian Research and Development Foundation, Research Corporation, Texas Advanced Research Program, and the Alexander von Humboldt Foundation.

[1] J. Pumplin *et al.*, JHEP **0207**, 12 (2002);
    D. Stump *et al.*, JHEP **0310**, 046 (2003).
[2] DØ Collaboration, F. Last, Nucl. Instrum. Methods A **123**, 456 (2004).
[3] CDF Collaboration, A. Abulencia *et al.*, hep-ex/0512020 (2006)
[4] D0 Collaboration, B. Abbot *et al.*, Phys. Rev. Lett. **82**, 2451 (1999).
[5] CDF Collaboration, F. Abe *et al.*, Phys. Rev. Lett. **77**, 438 (1996).
[6] G. C. Blazey *et al.*, in *Proceedings of the Workshop: "QCD and Weak Boson Physics in Run II"*, edited by U. Baur, R. K. Ellis, and D. Zeppenfeld, Batavia, Illinois (2000) p. 47. See Section 3.5 for details.
[7] T. Sjöstrand *et al.*, Comp. Phys. Comm. **135**, 238 (2001).
[8] Z. Nagy, Phys. Rev. Lett. **88**, 122003 (2002);
    Z. Nagy, Phys. Rev. D **68**, 094002 (2003).
[9] T. Kluge, K. Rabbertz, M. Wobisch, publication in preparation, http://hepforge.cedar.ac.uk/fastnlo/
[10] A.D. Martin *et al.*, Phys. Lett. B604, 61 (2004)
[11] N. Kidonakis, J.F. Owens, Phys. Rev. D63, 054019 (2001)
[12] S. Alekhin, Phys.Rev.D68:014002 (2003).
[13] G. Marchesini *et al.*, Comp. Phys. Comm. **67**, 465 (1992); G. Corcella *et al.*, JHEP **0101**, 010 (2001).
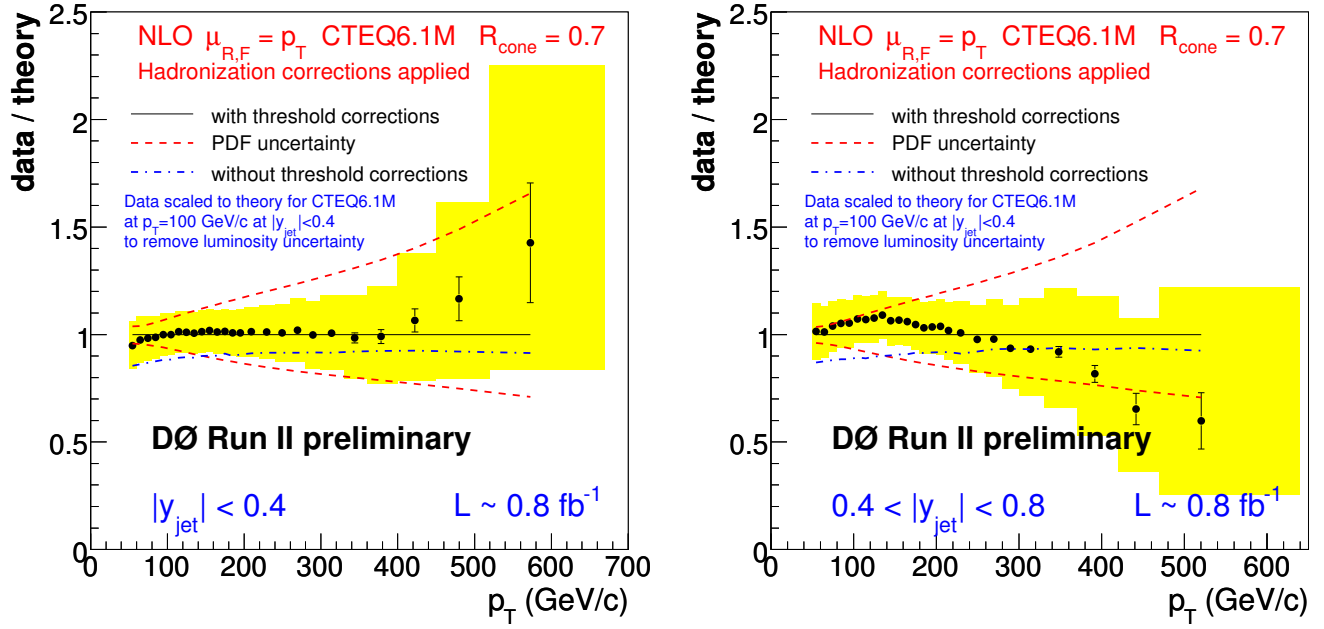
FIG. 7: The ratio of the measured inclusive jet cross section and the pQCD predictions are corrected for hadronization effects in two regions of jet rapidity. The systematic experimental uncertainty is shown by the shaded band. The NLO prediction without thresholds corrections are shown as the dash-dotted line. The uncertainty due to the CTEQ6.1M PDFs is indicated by the dashed lines.
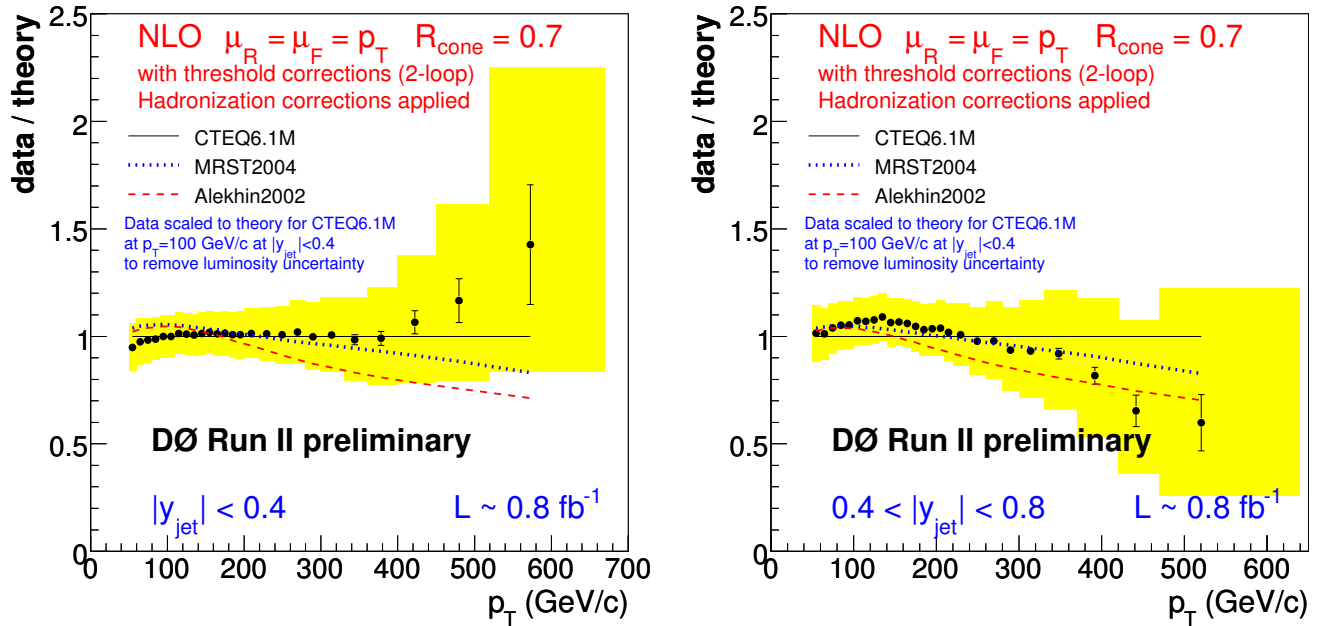

FIG. 8: The ratio of the measured inclusive jet cross section and the pQCD predictions corrected for hadronization effects in two regions of jet rapidity. The systematic experimental uncertainty is shown by the shaded band. The predictions for MRST2004 and Alekhin2002 PDFs, divided by the prediction for CTEQ6.1M, are shown as the dotted and dashed lines, respectively.
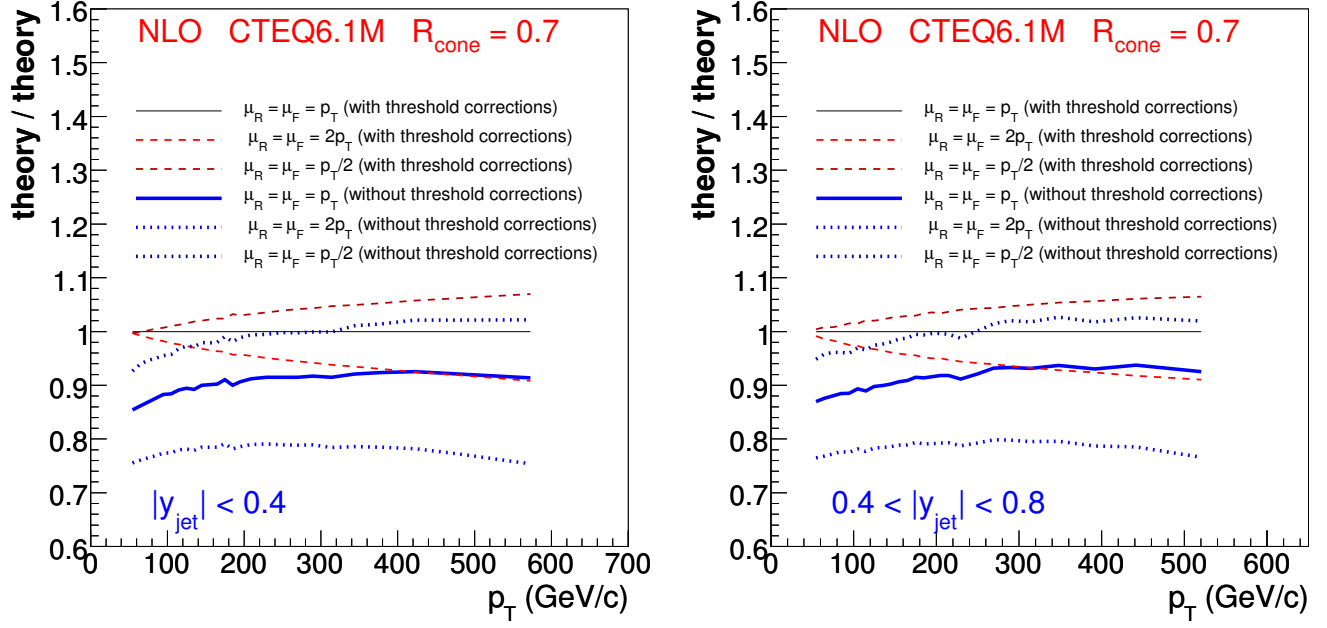
FIG. 9: The ratio of the NLO pQCD prediction with and without threshold corrections in two regions of jet rapidity. The scale dependence of calculations is indicated by the dashed (with threshold corrections) and dotted (without threhold corrections) lines.

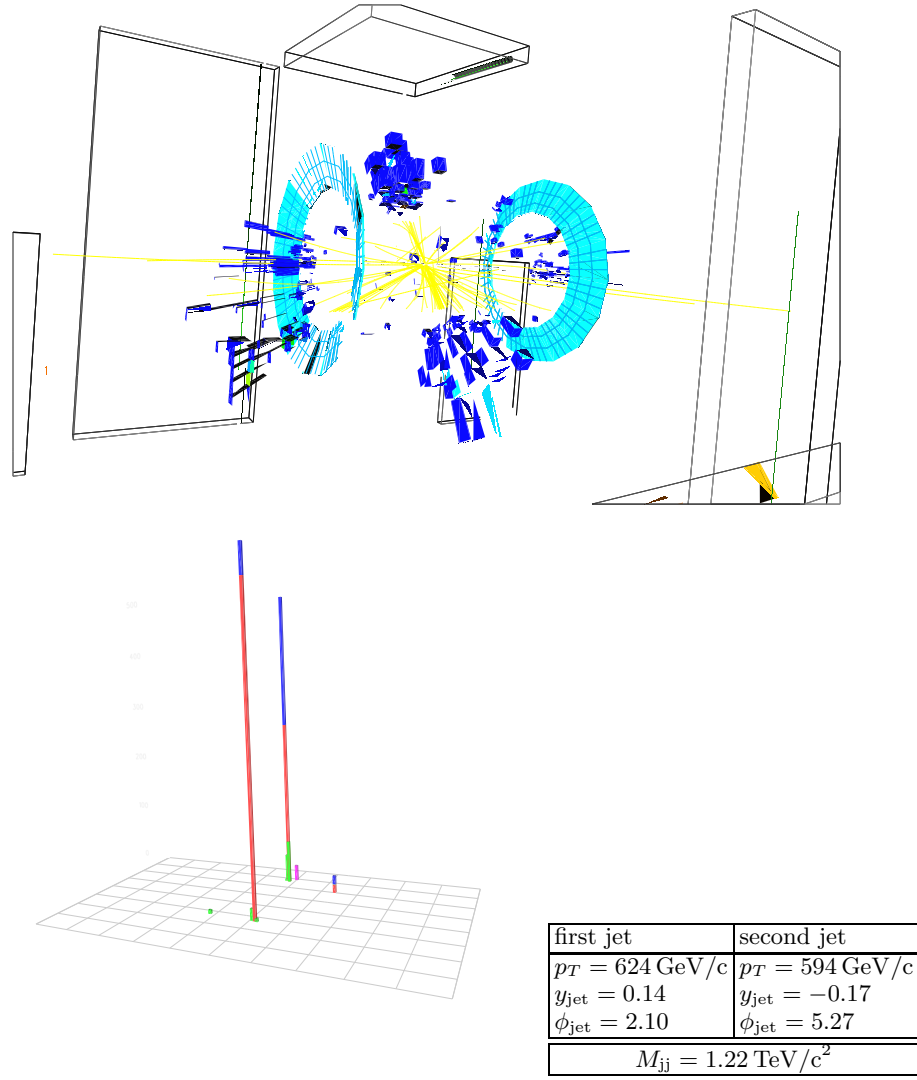| first jet	second jet
$p_T = 624\,\mathrm{GeV/c}$	$p_T = 594\,\mathrm{GeV/c}$
$y_{\mathrm{jet}} = 0.14$	$y_{\mathrm{jet}} = -0.17$
$\phi_{\mathrm{jet}} = 2.10$	$\phi_{\mathrm{jet}} = 5.27$
$M_{\mathrm{jj}} = 1.22\,\mathrm{TeV/c^2}$	

FIG. 10: Different views of the event that contains the jet with highest transverse momentum in the data sample.